J. Condensed Matter Nucl. Sci. 29 (2019) 440–452

Research Article

Resonant Surface Capture Model

Xingzhong Li*, Zhanmin Dong, Changlin Liang and Guisong Huang

Department of Physics, Tsinghua University, Beijing, China

Abstract

A resonant surface capture model is proposed to explain the various phenomena: the temperature dependence of excess heat, nuclear fusion cross-section data from beam–target experiments and from condensed matter nuclear reactions. This model is based on Oppenheimer's stripping nuclear reaction, and Bethe's solar energy calculation using the resonance effect to put the incoming projectile at the edge of target nucleus without forming compound nucleus. This is a new kind of resonance at low energy: the width of which is proportional to $E_0^{3/2}$ instead of $\exp\left[-\frac{C}{\sqrt{E_0}}\right]$, when the resonance energy $E_0 \to 0$.
 ISSN 2227-3123

Keywords: Lithium–hydrogen fusion reaction, 3-Parameter formula for fusion cross-section, Resonant surface capture model, Temperature dependence of excess heat, Width of resonance

1. Introduction – The Concept of Resonant Surface Capture

In 2016, Storms [1] published an important discovery: the temperature dependence of excess heat is a straight line in the semi-logarithmic plot (Fig. 1, blue dotted line), and the slope of this straight line is close to the activation energy (E_a) of the diffusion coefficient. At a first glance, it was a big surprise: the excess heat is an inelastic nuclear scattering process, but the diffusion is an elastic nuclear scattering process. How can be related to each other? What is hidden behind this experimental phenomenon?

This phenomenon reveals an important role of the nuclear resonance. During the elastic process, the resonance would be fully developed without any damping; then, the resonance would put the peak of the wave function at the edge between the nuclear potential well and the Coulomb barrier (Fig. 2, red line at $r = a$). The peak implies that the nucleon in the target nucleus would have a chance to direct interact with the nucleon in the projectile, because the nucleons are sticking together and inside the range of nuclear interaction due to resonance. This is a surface capture process that occurs without forming a compound nucleus. The reaction energy would be carried away by the charged nuclear products, and be transferred to the surrounding electrons as excess heat. Thus an inelastic nuclear scattering process follows an elastic nuclear scattering due to the resonance. Two different processes are thus connected together by the resonance effect. We may call this model as resonant surface capture model.

*Corresponding author. E-mail: lxz-dmp@tsinghua.edu.cn.

 ISSN 2227-3123

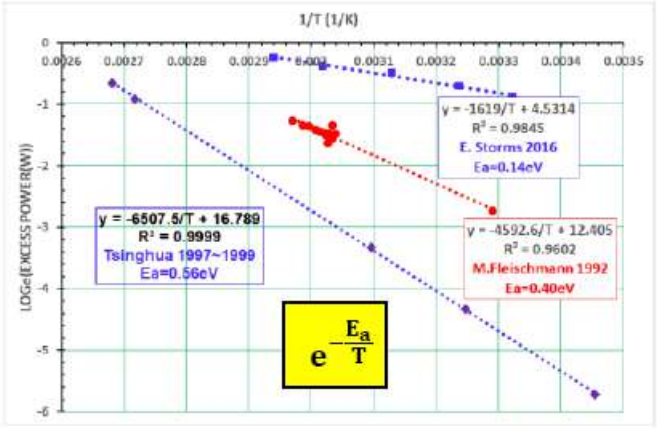

Figure 1. The temperature dependence of excess is a straight line in semi-logarithmic plot.

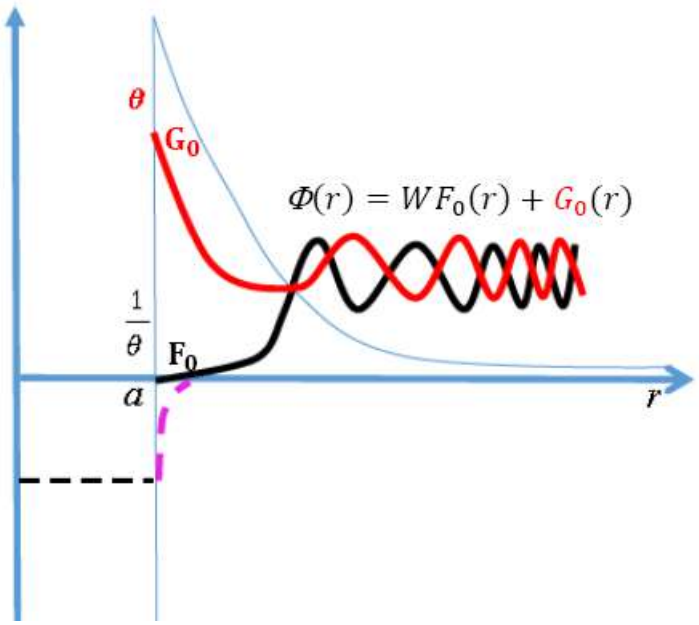

Figure 2. The resonance makes the wave function peaked at the edge of nuclear potential well (*red line*).

This direct nuclear interaction is very similar to the nuclear stripping interaction proposed by Oppenheimer in 1935 [2], and justified by the experimental data. The only new feature here is the resonance which put the projectile at the edge of the target nucleus. This process does not excite the target to a highly excited nuclear state; therefore, there would be no strong Gamma radiation accompanying this excess heat.

2. Equation – Resonance appears when $|W| \leq 1$ Instead of $W = 0$

The concept of resonant surface capture may be expressed by a peaked wave function inside a Coulomb field which is connected to the nuclear potential well (thin blue line in Fig. 2). In quantum mechanics any wave function, $\Phi(r)$, inside a Coulomb field may be expressed by a linear combination of two independent solutions of Schrodinger equation as:

$$\Phi(r) = WF_0(r) + G_0(r). \tag{1}$$

Here, $\Phi(r)$ is the reduced radial wave function of the relative motion between injected projectile and the target nucleus; $F_0(r)$ and $G_0(r)$ are the regular and irregular Coulomb wave functions for zero orbital angular momentum, respectively, because we are only interested in the low energy case. When $r \to a$, $F_0(r)$ decreases rapidly to a very small number in order of $\frac{1}{\theta}$ (lower black solid line in Fig. 2) and $G_0(r)$ increases rapidly to a very large number in order of θ (upper red solid line in Fig. 2). θ depends on energy exponentially as:

$$\theta = \sqrt{\frac{e^{2\pi\eta} - 1}{2\pi}}, \tag{2}$$

θ^2 is the Coulomb barrier factor which is similar to the reciprocal of Gamow factor; and $\eta \equiv \frac{1}{k\,a_c}$ – the Coulomb variable;

$$a_c \equiv \frac{4\pi\epsilon_0\hbar^2}{\mu Z_1 Z_2 e^2},$$

the Coulomb unit of length and k is the momentum of relative motion between projectile and target nucleus

$$k \equiv \sqrt{\frac{2\mu E}{\hbar^2}}$$

and E is the energy of this relative motion in the center of mass system. $Z_1 e$ and $Z_2 e$ are their electrical charges, μ is the reduced mass, ϵ_0 the dielectric constant of vacuum, $\hbar$ is the Planck constant divided by 2π. It is interesting to notice that: Although $|F_0(r)||_{r=a} \ll |G_0(r)||_{r=a}$, the logarithmic derivative of $F_0(r)$ and $G_0(r)$ at $r = a$ are similar in magnitude [3], i.e.

$$\left|\frac{1}{F_0(r)}\frac{\partial F_0(r)}{\eth r}\right|_{r=a} \approx \left|\frac{1}{G_0(r)}\frac{\partial G_0(r)}{\eth r}\right|_{r=a}, \quad \text{when } k \ll \sqrt{\frac{2}{a\,a_c}}. \tag{3}$$

This feature of $F_0(r)$ and $G_0(r)$ at $r = a$ makes the coefficient of the linear combination, W, extremely large in most cases because the wave function has to be connected smoothly to the wave function inside the nuclear potential well. The logarithmic derivative of wave function $\Phi(r)$ at $r = a$ must equal to D_L, the logarithmic derivative of wave function inside the nuclear potential well. It makes W very large at low energy, because

$$W = -\frac{G_0(a)}{F_0(a)}\left[\frac{D_L - \frac{1}{G_0(r)}\frac{\partial G_0(r)}{\eth r}}{D_L - \frac{1}{F_0(r)}\frac{\partial F_0(r)}{\eth r}}\right]_{r=a} = -\theta^2\left[\left(\frac{a_c}{a}\right)\frac{D_L - \frac{1}{G_0(r)}\frac{\partial G_0(r)}{\eth r}}{D_L - \frac{1}{F_0(r)}\frac{\partial F_0(r)}{\eth r}}\right]_{r=a}, \tag{4}$$

and θ^2 is a very large number at low energy. While θ^2 is known, the factor in square bracket in Eq. (4) is unknown, because it involves unknown nuclear property, D_L .

Figure 2 is plotted for the case of W=1. Usually, we think that when the factor in square bracket in Eq. (4) makes $W = 0$; then, there will be only $G_0(r)$ in Eq. (1), and the wave function, $\Phi(r)$, would be peaked at the boundary between Coulomb field and nuclear potential (Fig. 2 upper red solid line). So the resonant phenomenon would appear at $W = 0$. However, even if $W \neq 0$, provided that $|W| \leq 1$, we may still have a wave function,$\Phi(r)$, peaked at the boundary between Coulomb field and nuclear potential as shown in Fig. 2. Therefore, in order to study the resonant scattering, we should find the energy dependence of W, and search the pair of nuclei which makes $|W| \leq 1$.

3. A Tool for Finding Energy Dependence of W – 3-Parameter Formula for Fusion Cross-section

In quantum mechanics, W is directly related to low energy fusion cross-section as [4–10]:

$$\sigma_{\text{Fusion}}(E) = \frac{\pi}{k^2} \frac{(-4W_{\text{i}})}{(W_{\text{r}})^2 + (1 - W_{\text{i}})^2}. \tag{5}$$

Here W_{r} and W_{i} are the real and imaginary parts of W. Equation (5) gives a tool to determine the W from the experimental data of fusion cross-section, $\sigma_{\text{Fusion}}(E)$. Equation (4) has shown that W might be separated into two factors: the Coulomb field factor, θ^2, which is known as a real number by Eq. (2), and the remaining complex nuclear factor. We may rewrite the W as

$$W \equiv \theta^2(w_{\text{r}} + w_{\text{i}}). \tag{6}$$

The Coulomb field factor θ^2, varies rapidly with energy; and the unknown nuclear factor, $(w_{\text{r}} + w_{\text{i}})$, might be found through low energy fusion cross-section data. From the d + T $\rightarrow$ n + ^{4}He fusion cross-section, we have found that w_{r} varies slowly with energy, and w_{i} is almost a constant at low energy. The d + T fusion cross-section may thus be expressed by a 3-parameter formula very well:

$$W_{\text{r}} = \theta^2(C_1 + C_2E), \quad W_{\text{i}} = \theta^2 C_3, \tag{7}$$

$$\sigma_{\text{Fusion}}(E) = \frac{\pi}{k^2} \frac{(-4C_3)}{\theta^2[(C_1 + C_2E)^2 + \left(\frac{1}{\theta^2} - C_3\right)^2]}. \tag{8}$$

Figure 3 gives the comparison between this 3-parameter formula and the experimental data. Here the black circles are experimental data from the National Nuclear Data Center (ENDF/B-VIII.0) [11]. The red lines are from 3-parameter formula, Eq. (8). In order to show the good fit, both logarithmic scale (left axis) and linear scale (right axis) are plotted to show the fit from 200 eV to 200 keV [12].

Indeed, Eq. (8) has been justified by more than 15 pairs of fusion cross-section data. It gives two important features of W: (i) W_{r} and W_{i} are the products of θ^2 and a constant at very low energy, respectively. (ii) At very low energy both W_{r} and W_{i} are extremely rapidly decreasing when energy is increasing, because θ^2 is an extremely rapidly decreasing function when energy is increasing as expressed by Eqs. (2)–(4). When $k \rightarrow 0$, $\eta \rightarrow \infty$; then, $\theta^2 \rightarrow \infty$ exponentially. On the other hand, when $k \rightarrow \infty$, $\eta \rightarrow 0$; then, $\theta^2 \rightarrow \eta \rightarrow 0$. These two features imply that there must be an energy, E_0, above which both W_{r} and W_{i} are less than 1. Moreover, if this resonance energy, E_0, is low enough; then, we may show that the resonant *elastic* nuclear scattering cross-section would be a *step-wise* function of energy E due to the rapid variation of θ at low energy.

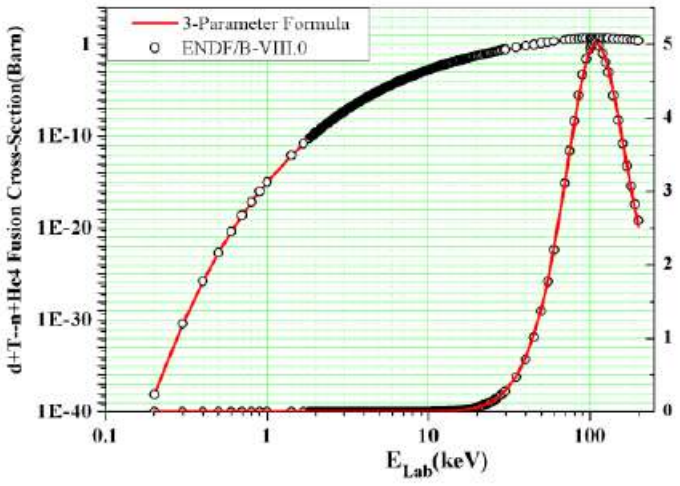

Figure 3. d+T→n+ ^{4}He fusion cross-section data reveal energy dependence of *W*.

4. Low-energy Resonant Elastic Nuclear Scattering Cross-Section – A Step-wise Function of Energy *E*

In quantum mechanics, the elastic scattering cross-section is expressed by W as well [13]

$$\sigma_{\text{Elastic}}(E) = \frac{\pi}{k^2}\frac{4}{(W_{\text{r}})^2 + (1 - W_{\text{i}})^2}. \tag{9}$$

When energy is greater than the resonant energy. E_0 , both $W_r \text{and} W_i \text{are}$ less than 1; then

$$\sigma_{\text{Elastic}}(E) = \frac{\pi}{k^2}\frac{4}{(W_{\text{r}})^2 + (1 - W_{\text{i}})^2} \to \frac{4\pi}{k^2}. \tag{10}$$

When energy is less than the resonant energy. E_0, both $W_{\text{r}} \text{and} W_{\text{i}} \text{are}$ rapidly increasing to be greater than 1; then

$$\sigma_{Elastic}(E) = \frac{\pi}{k^2}\frac{4}{(W_r)^2 + (1 - W_i)^2} \propto \frac{4\pi}{k^2\theta^4} \to 0. \tag{11}$$

We may illustrate this behaviour by assuming two resonance energy, $E_{0\text{r}}$ and $E_{0\text{i}}$ for W_{r} and W_{i}, respectively:

$$W_{\text{r}} = \frac{\theta(E)^2}{\theta(E_{0\text{r}})^2}\left(1 - \frac{E}{E_{0\text{r}}}\right) \text{ and } W_{\text{i}} = \frac{\theta(E)^2}{\theta(E_{0\text{i}})^2}. \tag{12}$$

This assumption gives:

$$W_{\text{r}} = 0 \quad \text{at} \quad E = E_{0\text{r}}, \tag{13}$$

$$W_{\text{r}}^2 \gg 1, \quad \text{when } E \ll E_{0\text{r}} \text{ and } W_{\text{r}}^2 \ll 1, \quad \text{when } E \gg E_{0\text{r}}, \tag{14}$$

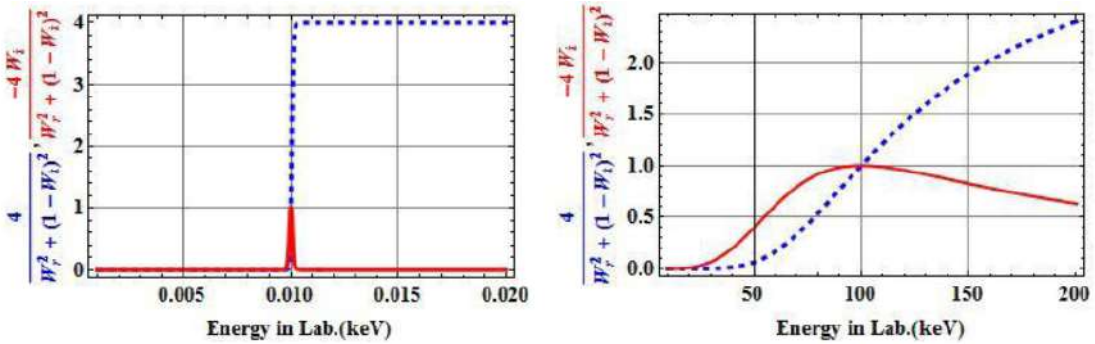

Figure 4. Changing from $E_0 = 100$ keV (*right*) and $E_0 = 10$ eV (left) shows that blue dotted line becomes a step-wise line, and red line becomes a peak-wise line.

$$W_{\rm i}^2 \gg 1, \quad \text{when } E \ll E_{0\rm i} \text{ and } W_{\rm i}^2 \ll 1, \quad \text{when } E \gg E_{0\rm i}. \tag{15}$$

In Fig. 4, the blue dotted line shows the factor

$$\frac{4}{(W_{\rm r})^2 + (1 - W_{\rm i})^2}$$

as a function of energy for two cases: $E_{0\rm r} = E_{0\rm i} = E_0$ =100 keV, and $E_{0\rm r} = E_{0\rm i} = E_0$ =10 eV. It is evident that the blue dotted line becomes a step-wise function when E_0 is getting smaller. We may expect a much steeper line when E_0 approaches thermal energy (~25 meV).

5. Low-energy Resonant Inelastic Nuclear Scattering Cross-Section – A Peak-wise Function of Energy *E*

According to resonant surface capture model, the cross-section of nuclear reaction is a transition after this resonant elastic scattering [2,14]; hence,

$$\sigma_{\text{Surface capture}}(E) = \frac{\pi}{k^2} \frac{4}{(W_{\rm r})^2 + (1 - W_{\rm i})^2} \left[\int \psi_{\rm f}^* H_{\rm int} \psi_{\rm i} \, {\rm d}\tau \right]^2, \tag{16}$$

Here,

$$\left[\int \psi_{\rm f}^* H_{\rm int} \psi_{\rm i} \, {\rm d}\tau \right]^2$$

is the transition probability from the initial state, $\psi_{\rm i}$, to the final state, $\psi_{\rm f}$. The initial state, $\psi_{\rm i}$, is a plane wave at $r \to \infty$ formed by the incoming projectile and the target nucleus; and the final state, $\psi_{\rm f}$, is a halo state formed by the captured nucleon in the halo of target nucleus (purple dotted line in Fig. 2). This transition happen only if the overlapping between $\psi_{\rm i}$ and $\psi_{\rm f}$ is not negligible. $\psi_{\rm f}$ decreases rapidly when $r > a$; hence, the overlapping integration becomes not negligible only if $\psi_{\rm i}$ is large at the edge $r = a$, i.e. in the case of resonance when G_0 is dominant in the linear combination. Thus $\psi_{\rm i} \propto G_0 \propto \theta$. Or

$$\sigma_{\text{Surface capture}}(E) = \frac{\pi}{k^2} \frac{4}{(W_{\rm r})^2 + (1 - W_{\rm i})^2} \left[\int \psi_{\rm f}^* H_{\rm int} \psi_{\rm i} \, {\rm d}\tau \right]^2 \propto \frac{\pi}{k^2} \frac{4}{(W_{\rm r})^2 + (1 - W_{\rm i})^2} \theta^2, \tag{17}$$

when energy is greater than the resonant energy. E_0, both W_r and W_i are less than 1; then

$$\sigma_{\text{Surface Capture}}(E) = \frac{\pi}{k^2}\frac{4}{(W_\mathrm{r})^2 + (1 - W_\mathrm{i})^2}\theta^2 \to \frac{4\pi}{k^2}\theta^2, \tag{18}$$

when energy is less than the resonant energy. E_0, both W_r and W_i are rapidly increasing to be greater than 1; then

$$\sigma_{\text{Surface Capture}}(E) = \frac{\pi}{k^2}\frac{4}{(W_\mathrm{r})^2 + (1 - W_\mathrm{i})^2}\theta^2 \to \frac{4\pi}{k^2\theta^4}\theta^2 \to 0, \tag{19}$$

In Fig. 4, the red solid line shows the factor

$$\frac{4}{(W_\mathrm{r})^2 + (1 - W_\mathrm{i})^2}\theta^2$$

as a function of energy with E_0 =10 eV (having assumed both W_r and W_i are equal to 1 at same energy E_0). The additional factor, θ^2, in numerator adds a steep decreasing behaviour in the region where $E > E_0$. Thus the resonant surface capture cross-section becomes a peak-wise function with peak at $E \approx E_0$. We may expect much more sharp peak behavior when E_0 approaches thermal energy (~25 meV).

6. Average Over Maxwell Distribution Function

In order to study the temperature dependence of excess heat and diffusion in Fig. 1, we have to average the collision rate over the Maxwell velocity distribution. For the elastic collision rate,

$$\langle \sigma_{\text{Elastic}}\, v\rangle = \left(\frac{\mu}{2\pi k_\mathrm{B}T}\right)^{3/2}\int_0^\infty \left(\frac{\pi}{k^2}\frac{4}{W^2+1}\right) v \exp\left[-\frac{\mu v^2}{2k_\mathrm{B}T}\right] 4\pi v^2\,\mathrm{d}v \propto \int_{E_0}^\infty \exp\left[-\frac{E}{T}\right]\mathrm{d}E \propto \exp\left[-\frac{E_0}{T}\right]. \tag{20}$$

The step-wise behaviour of $4/(W^2 + 1)$ just changes the lower limit of integration from 0 to E_0 , it results an exponential factor, $\exp[-(E_0/T)]$.

For the resonant surface capture rate, this same exponential factor will appear as well:

$$\begin{aligned}\langle \sigma_{\text{Excess Heat}}\, v\rangle &= \left(\frac{\mu}{2\pi k_\mathrm{B}T}\right)^{3/2}\int_0^\infty \left(\frac{\pi}{k^2}\frac{4}{W^2+1}\right)\left|\int \psi_\mathrm{f}^* H_{\text{int}}\Psi_\mathrm{i}\,\mathrm{d}\tau\right|^2 v\exp\left[-\frac{\mu v^2}{2k_\mathrm{B}T}\right]4\pi v^2\,\mathrm{d}v \\ &\propto \int_0^\infty \frac{4}{W^2+1}\theta^2\exp\left[-\frac{E}{T}\right]\mathrm{d}E \propto \exp\left[-\frac{E_0}{T}\right]\Delta E.\end{aligned} \tag{21}$$

The peak-wise behavior of

$$\frac{4}{W^2+1}\theta^2$$

just turns the integration into the product of $\exp[-E_0/T]$, and ΔE, i.e. the peak value of integrand at E_0 times the energy width ΔE.

Now we have shown that both the elastic collision rate and the resonant surface capture rate share the same exponential factor $\exp[-E_0/T]$ as shown in Fig. 1. Indeed it gives the hint that there must be a low-energy resonance at the energy E_0 which is close to the activation energy of diffusion coefficient, E_a .

7. Comparison with More Experimental Data

In addition to the theoretical derivation of Storms' straight line, we would like to see if there is any more experimental evidences to support this behavior. The first such evidence may be Fleischmann and Pons' famous "Heat after Death" experiment in 1992 [15]. Before the electrolyte reached the boil point, there were 12 data points for excess heat power at certain temperatures. In Fig. 1, the red dotted line goes just along with these 12 red points. Only a few points after the triggering are not on this straight dotted line. However, the slope of this straight line is different from that of Storms' blue dotted line which is thought to be the activation energy of deuteron diffusion coefficient in palladium. Then what is the possible reason for this difference? As we remember, Fleischmann and Pons would like to add LiOD in the electrolyte in order to enhance the conductivity of electrolyte for obtaining greater current density which was believed to be an important condition to have excess heat at those early days. As mentioned by Storms, after long time of electrolysis there was a possibility of forming lithium–palladium alloy in the cathode surface. Therefore, we might think the activation energy of deuteron diffusion in lithium deuteride. The search in literature did not give the activation energy for deuteron diffusion in LiD in the temperature range of interests. The only available activation energy in this temperature range is for lithium diffusion in LiH, i.e. E_{a}= 38.5 kJ/mol= 4632 K (~0.399 eV) [16], it is very close to the slope of that red dotted line in Fig. 1 (4593 K~0.396 eV). According to literature [16], the activation energy of D in LiD (or H diffusion in LiH) is expected to be close to $38.5\mathrm{kJ/mol}$ in the temperature range of interests. More experimental data are desirable.

Having been encouraged by this comparison, we re-examined Tsinghua University data from gas-loading experiments performed early in 1996–1999 [17,18]. The purple dotted line in Fig. 1 shows another good fit with experimental data points. It seems that both in gas-loading and in electrolysis experiments, the temperature dependence of excess heat is a straight line in the semi-logarithmic plot, and there should be a low energy resonance between deuteron (or proton) and some target nucleus. We would like to address the possible target nucleus here for electrolysis experiments and shall discuss this gas-loading straight line in another proceedings paper [19].

8. The Evidences of Low-energy Resonance for Nuclear Reaction

From 3-parameter formula for fusion cross-section Eq. (8), it is possible to find the low-energy resonance as well. If there is a low-energy resonance at $E = E_0$ for elastic scattering; then, the rapidly decreasing θ^2 would make $\theta^2[(C_1 + C_2E)^2] \to 0$ in the region $E > E_0$. Since most of fusion cross-section data are taken from beam–target experiments using accelerator, the beam energy is greater than the resonance energy, E_0, which is supposed to be near thermal energy. Thus we may expect that the fusion cross-section would be fit by only one parameter, C_3, as

$$\sigma_{\text{Fusion}}(E) = \frac{\pi}{k^2}\frac{(-4C_3)}{\theta^2[(C_1 + C_2E)^2 + \left(\frac{1}{\theta^2} - C_3\right)^2]} \to \frac{\pi}{k^2}\frac{(-4C_3)}{\theta^2[\left(\frac{1}{\theta^2} - C_3\right)^2]} \to \frac{\pi}{k^2}\frac{(-4C_3\theta^2)}{(1 - C_3\theta^2)^2}. \tag{22}$$

Figure 5 shows the fusion cross-section for p + ^{6}Li $\to$ ^{3}He + ^{4}He. Black points are from ENDF/B-VIII.0, and the red line is from Eq. (22) with only one parameter $C_3 = -5.62$. The left and right axes are for logarithmic and linear scale, respectively, to show the good fit ($R^2 = 0.99999$). Indeed the existence of low energy resonance for p + ^{6}Li $\to$ ^{3}He + ^{4}He is provided by Lipinski's patent as well [20].

Figure 6 shows the fusion cross-section for d + ^{6}Li $\to$ ^{4}He + ^{4}He. Black points are from ENDF/B-VIII.0, and the red line is from Eq. (22) with only one parameter $C_3 = -0.1768$. The left and right axes are for logarithmic and linear scale, respectively, to show the good fit ($R^2 = 0.99997$). Indeed the existence of low-energy resonance for d + ^{6}Li $\to$ ^{4}He + ^{4}He is provided by Pons' heavy water electrolysis experiment using enriched ^{6}LiOD as well. After long period of electrolysis using palladium cathode Pons observed a big amount of helium with excess heat [21].

These experiments just explain the slope of red straight line in Fig. 1.

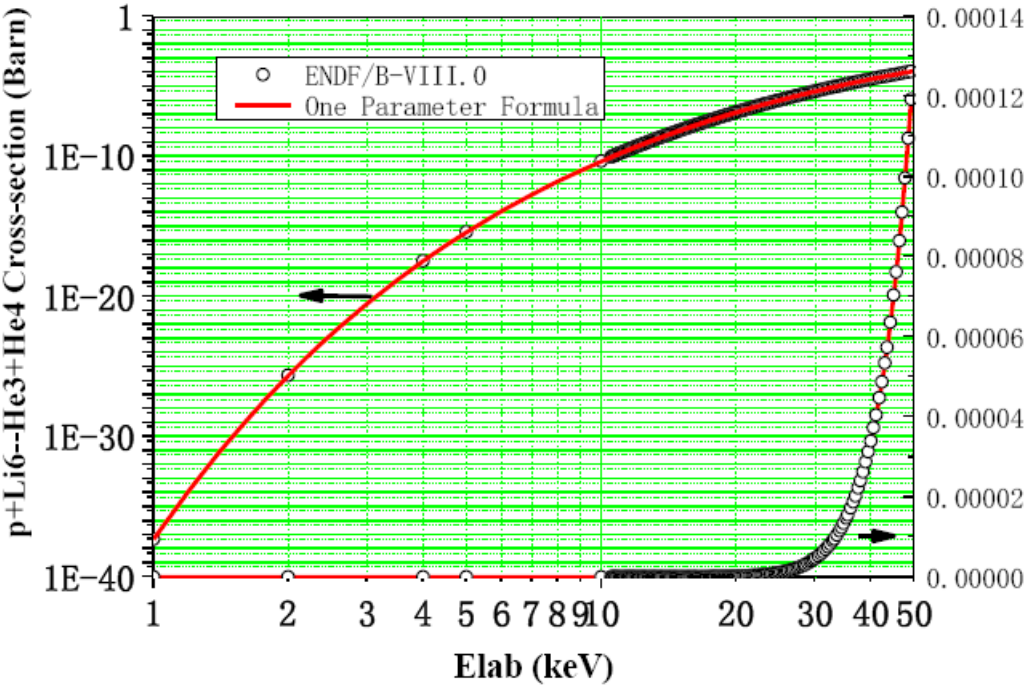

Figure 5. $\mathrm{p} + {}^{6}\mathrm{Li} \rightarrow {}^{3}\mathrm{He} + {}^{4}\mathrm{He}$ fusion reaction cross-section at low energy may be fit by 1-parameter formula.

9. Two Kinds of Resonance Widths

The widths of peaks in Fig. 3 (at 100 keV) and in the integrand of Eq. (21) are very different, because the resonance peak in Fig. 3 is determined by $W_{\mathrm{r}} = 0$, and the resonance peak in the integrand of Eq. (21) for a transition after the ***pure*** elastic collision is determined by $W = W_{\mathrm{r}} = 1$.

Since the Coulomb barrier factor

$$\theta = \sqrt{\frac{\mathrm{e}^{2\pi\eta} - 1}{2\pi}} \approx \sqrt{\frac{\mathrm{e}^{31.4Z_1Z_2\sqrt{\frac{m_1}{E_{\text{lab keV}}}}}}{2\pi}},$$

the changing rate of θ^2 would be much slower when

$$E_{\text{lab keV}} > \left(\frac{31.4Z_1Z_2\sqrt{m_1}}{2}\right)^{2/3}.$$

Here, $E_{\text{lab keV}}$ is the kinetic energy of the injected projectile in laboratory system in unit of keV, m_1 is its mass number (an integer),

$$\left(\frac{31.4Z_1Z_2\sqrt{m_1}}{2}\right)^{2/3} \approx 7.9 \text{ keV}$$

for d+T fusion. This affects the width of resonance peak.

The resonance peak in Fig. 3 for d+T fusion is near 100 keV which is greater than

$$\left(\frac{31.4Z_1Z_2\sqrt{m_1}}{2}\right)^{2/3}.$$

therefore, the variation of $W_r \equiv \theta^2 w_r$ around 100 keV is mainly determined by $w_r = C_1 + C_2E$. The width would be determined by

$$\Delta E_h \approx \frac{2}{\theta^2 C_2} \quad \text{at} \quad E_{0h} = -\frac{C_1}{C_2} \quad \text{where} \quad w_r = 0.$$

This expression may give a wrong impression that the width of resonance would be extremely small as

$$\Delta E_h \to \left|\frac{2}{\theta^2 C_2}\right|_{E_{\text{lab keV}}\to 0} \to 0.$$

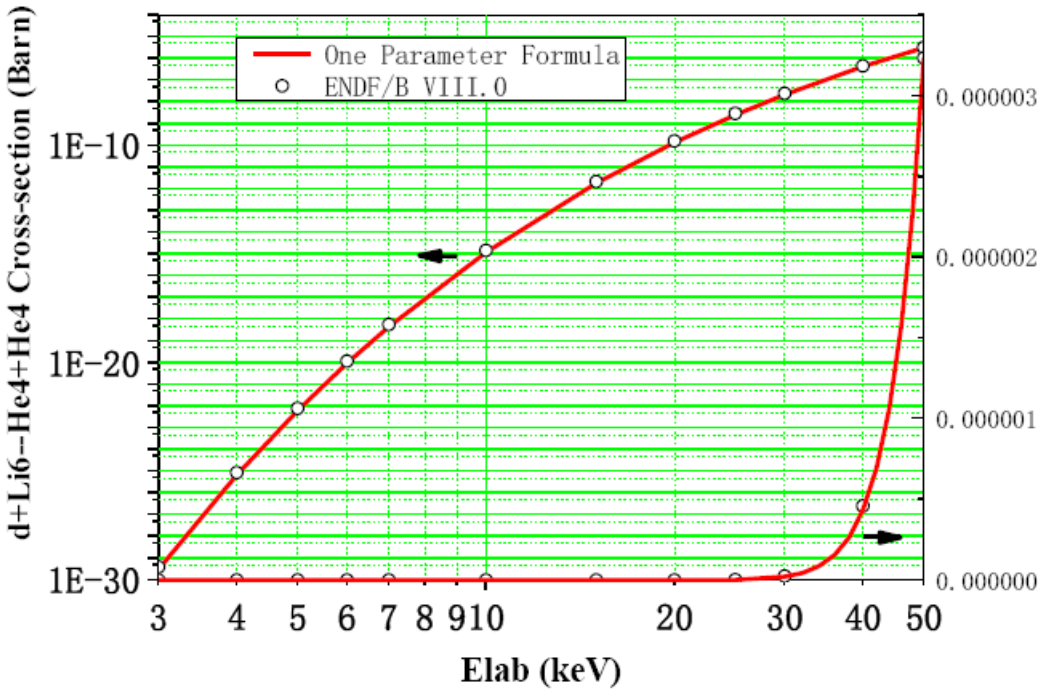

Figure 6. $d + {}^6Li \to {}^4He + {}^4He$ fusion reaction cross-section at low energy may be fit by 1-parameter formula.

This is not true, for $E_{\text{lab keV}} \to 0$. Indeed in the integrand of Eq. (21) for a transition after the ***pure*** elastic collision (where a resonance energy is supposed to be $E_{0\text{lab keV}} < 0.01\text{keV}$), $E_{0\text{lab keV}}$ is much smaller than

$$\left(\frac{31.4Z_1Z_2\sqrt{m}_1}{2}\right)^{2/3} \quad \left(\text{for p} +^6 \text{Li fusion} \quad \left(\frac{31.4Z_1Z_2\sqrt{m}_1}{2}\right)^{2/3} \approx 13\,\text{keV}\right)$$

therefore, the variation of $W_\text{r} \equiv \theta^2 w_\text{r}$ around 0.01 keV in the integrand of Eq. (21) is mainly determined by θ^2 instead of w_r (because at this low energy, $w_\text{r} \to C_1 =$ constatnt). The width of resonance peak would be determined by the peak-wise behavior of $\frac{4}{W^2+1}\theta^2$. The step-wise denominator determines the up-slop behavior of the peak at $E_{0\text{c}}$ with

$$w_\text{r} = \frac{1}{\theta(E_{0\text{c}})^2} \quad (\text{i.e. } W = W_\text{r} = 1),$$

and the θ^2 in numerator determines the down-slop of peak with a width of

$$\Delta E_{0\text{c}} \approx \frac{2\,\text{Log}\frac{1}{2}}{31.4Z_1Z_2\sqrt{m}_1}(E_{0\text{Labk eV}})^{3/2} \quad \left(\text{i.e. } \theta[E_{0\text{c}} + \Delta E_{0\text{c}}]^2 = \frac{1}{2}\theta[E_{0\text{c}}]^2\right).$$

Although the energy width $\Delta E_{0\text{c}}$ still goes to zero, when $E_{0\text{Lab keV}} \to 0$, it is much more slower than $\frac{1}{\theta^2}$. This resonance peak at low energy will have enough contribution to the integration in Eq. (21).

10. Conclusion

The essence of resonance is to put the wave peak at the edge of the nuclear boundary; then, Coulomb repulsion becomes Coulomb *attraction*. Once the injected projectile sticks on the surface of target nucleus, the nucleons near the surface are in the range of the strong interaction even if no compound nucleus is formed.

This effect was justified by Oppenheimer (1935) [2] in terms of the angular distribution of nuclear products with energetic projectile (which are approximately several MeV). This resonant surface capture model only makes use of the resonance to put the projectile on the surface of the target nucleus. Indeed Bethe applied a similar calculation for the weak interaction $\text{p} + \text{p} \to \text{D} + \text{e}^+ +$ neutrino in the solar energy model [14]. Bethe included the resonance effect partly in his calculation, but the approximation in his simplification prevented him from fully considering the resonance effect. However, the overlapping of the initial wave function with the final wave function provided a good estimate of the transition probability both in Oppenheimer's stripping reaction and in Bethe's solar energy calculation.

Our new finding is a feature of low-energy resonance in condensed matter which is quite different from the resonance in beam–target experiments. The resonance energy, E_0, is no longer determined by the $W_\text{r} = 0$ in the denominator of Eq. (5), instead it is determined by $W_\text{r}^2 + W_\text{i}^2 \leq 1$. Therefore, the width of resonance is no longer decreasing as $1/\theta^2 \to 0$ at low energy, instead it is decreasing as $(E_{0\text{c}})^{3/2}$ which is much slower than $1/\theta^2$.

The slope of straight lines in Storms' semi-logarithmic plot and the data from experiments (Beam–target data from the National Nuclear Data Center, Lipinski patent for "Low energy Hydrogen–Lithium Fusion Reactor", and Pons' electrolysis with enriched lithium (^{6}LiOD)) all point to ^{6}Li as a possible fuel candidate in Condensed Matter Nuclear Science.

The two-step resonant surface capture model explains not only the low energy nuclear reaction without Coulomb repulsion, but also the releasing of nuclear energy without strong Gamma and neutron radiation, because there were no highly excited nuclei involved in surface capture reaction (no compound nucleus formed).

We have to further find the collective mechanism in condensed matter which makes the resonant surface capture reaction happen on a large scale with a self-sustaining mode. Then a safe and clean nuclear energy source would be available to the whole world.

Acknowledgements

Many thanks to T. Passell for his guiding to lithium stripping reaction [22], to E. Storm for his discovery of temperature dependence of excess heat, to M. Miles for his thermodynamic derivation using Eyring theory [23], to A. Nicolas for his information about activation energy of H(D) diffusion in metals. This work is supported by The Ministry of Education (#20091770437), The Ministry of Science and Technology (Fundamental Research Division, #2009CB226113), Natural Science Foundation of China (#10475045 & #21153003) and Tsinghua University (Basic Research Fund (985-III)).

References

[1] E. Storms, How basic behavior of LENR can guide a search for an explanation, *J. Condensed Matter Nucl. Sci.* **20** (2016) 100–138.
[2] J.R. Oppenheimer and M. Phillips, Note on the transmutation function for deuterons, *Phys. Rev*. **48** (1935) 500–502. S.T. Butler, Direct nuclear reactions, *Phys. Rev*. **106** (1957), 272–286.
[3] M. Abramowitz and I.A. Stegun, *Handbook of Mathematical Functions*, 10th Printing, Dover, New York, p. 542 (14.6.9), December, 1972.
[4] X.Z. Li, Q.M. Wei and B. Liu, A new simple formula for fusion cross-sections of light nuclei, *Nucl. Fusion* **48** (2008) 125003.
[5] X.Z. Li, A new approach towards fusion energy with no strong nuclear radiation, *Nucl Fusion and Plasma Phys* **16** (2) (1996) 1–8 (in Chinese), see also *J. New Energy* **1** (4) (1996) 44–54 (in English).
[6] X.Z. Li, J. Tian, M.Y. Mei and C.X. Li, Sub-barrier fusion and selective resonant tunneling, *Phys. Rev.* C **61** (2000) 024610.
[7] X.Z. Li, Nuclear physics for nuclear fusion, *Fusion Sci. Technol.* **41** (2002) 63.
[8] X.Z. Li, B. Liu, S. Chen, Q.M. Wei and H. Hora, Fusion cross sections for inertial fusion energy, *Laser Part. Beams* **22** (2004) 469–477.
[9] X.Z. Li, Z.M. Dong and C.L. Liang, Studies on p+^{6}Li fusion reaction use 3-parameter model, *J. Fusion Energy* **31** (2012) 432–436.
[10] M. Kikuchi, *Frontiers in Fusion Research – Physics and Fusion*, Springer, London, 2011, p. 31.
[11] National Nuclear Data Center, Brookhaven National Laboratory, ENDF/B-VIII.0 (2018) is available on Internet http://www.nndc.bnl.gov.
[12] C.L. Liang, Z.M. Dong and X.Z. Li, Selective resonant tunneling – turning hydrogen-storage material into energetic material *Current Sci.* **108** (4) (2015) 519.
[13] L.D. Landau and E.M. Lifshitz *Quantum Mechanics*, 3rd. Edn.,revised and enlarged Reprinted 1991 (with corrections) p. 507.
[14] H.A. Bethe and C.L. Critchfield, The formation of deuterons by proton combination, *Phys. Rev.* **54** (1938) 248.
[15] M. Fleischmann, and S. Pons, Calorimetry of the Pd–D_2O system: from simplicity via complications to simplicity, *Phys. Lett*. A **176** (1993) 118.
[16] Hj. Matzke and V.V. Rondinella, Diffusion in carbides, nitrides, hydrides and borides 5.3 Diffusion in hydrides, Landolt –Börnstein, New Series III/33B1, pp. 5–49.
[17] Xing Z. Li, Bin Liu, Xian Z. Ren, Jian Tian, Wei Z. Yu, Dong X. Cao, Shi Chen, Guan H. Pan and Shu X. Zheng, Pumping effect – Reproducible excess heat in a gas-loading D/Pd system, in *The 9th Int. Conf. on Cold Fusion, Condensed Matter Nuclear Science*, 2002, Tsinghua University, Beijing, China, Tsinghua Univ. Press.
[18] Zhan M. Dong, Chang L. Liang, Bin Liu, Qing M. Wei, Jian Tian, Shu X. Zheng, Jin Z. Yu and Xing Z. Li, Studies on anomalous phenomena of D/Pd systems using a gas-loading process – a stride towards neutrino detection, *J. Condensed Matter Nucl. Sci.* **4** (2011) 119–131.

[19] Zhan M. Dong, Shu X. Zheng, Chang L. Liang and Xing Z. Li, Temperature dependence of excess heat in gas-loading experiments, appear in ICCF-21 proceedings paper.
[20] S.A. Lipinski and H.M. Lipinski, *Hydrogen–Lithium Fusion Device*, WO2014/189799 A9 (27 Nov. 2014).
[21] Private Communication (by J.-P. Biberian).
[22] T. Passell, The case for deuteron stripping with metal nuclei as the source of the Fleischmann–Pons excess heat effect, *J. Condensed Matter Nucl. Sci*. **15** (2014) 1–7.
[23] Melvin H. Miles and Iraj Parchamazad, The Eyring rate theory applied to cold fusion, presentation in SSICCF-20, Xiamen, China, Sept. 28–30, 2016 and in ICCF-20, Sendai, Japan, 2–7 October 2016.